ROSA: Reconstruction of Spectrogram Autocorrelation for Self-Amplified Spontaneous Emission Free-Electron Lasers

Svitozar Serkez[1], Oleg Gorobtsov[2,3], Bohdana Sobko[4], Natalia Gerasimova[1], and Gianluca Geloni[1]

[1]European XFEL GmbH, Hamburg, Germany
[2]Deutsches Elektronen-Synchrotron (DESY), Hamburg, Germany
[3]Present address: Department of Materials Science and Engineering, Cornell University, Ithaca, NY, USA
[4]Lviv National University, Lviv, Ukraine

November 29, 2018

Abstract

In recent years X-ray Free Electron Lasers (XFELs) proved to be unmatched sources of ultrashort pulses of spatially coherent quasimonochromatic X-ray radiation. Diagnostics of XFEL emission properties, in particular pulse duration, spectrum and temporal profile is extremely important in order to analyze the experimental results. In this paper we propose a cost-effective method to examine these properties of Self-Amplified Spontaneous Emission (SASE) pulses. It only requires an ensemble of measured SASE spectra and provides the temporal autocorrelation of the ensemble-averaged Wigner distribution of SASE FEL pulses.

1 Introduction

Free-electron laser sources provide high power, ultrashort pulses of narrow-bandwidth radiation at tunable wavelength [1–3].

In essence, a high-gain free electron laser is a combination of accelerator that produces a high-quality ultrarelativistic electron beam and undulator - a periodic magnetic structure where that beam is forced to oscillate transversely with respect to the main direction of motion. A positive feedback loop is formed in the undulator where electromagnetic field is amplified in an exponential fashion. A linear combination of electron density modulation, energy modulation and electromagnetic field present at the target wavelength provide initial conditions for the FEL process. Energy transfer from the electron beam to the electromagnetic radiation pulse is sustained when the resonance condition

$$\lambda = \lambda_u \frac{1 + K^2/2}{2\gamma^2} \tag{1}$$

is satisfied, where λ_u is the undulator period, γ is the Lorenz factor of the reference electron and $K = eH\lambda_u/2\pi m_e c^2$ is the undulator parameter, e is an electron charge, m_e - the electron rest mass, H - the maximum on-axis magnetic field and c - a speed of light in vacuum.

Note that if the average electron energy at the head of the beam differs significantly from that of the tail, the undulator resonance condition varies from head to tail, and the resulting radiation pulse is frequency chirped. We also remark that ideally, an electron beam should have a minimum energy spread and energy chirp to maximize the FEL gain and minimize the FEL bandwidth. Therefore, a monoenergetic electron beam is preferable to generate FEL radiation.

The electron beam phase space and the radiation output characteristics are closely related and difficult to diagnose.

X-band transverse deflecting radio-frequency cavities (XTCAV) [4] are powerful tools to directly measure the longitudinal phase space of FEL-class electron beams, allowing for the determination of the overall energy chirp, i.e. the correlated energy spread in the electron beam in order to minimize it. When installed downstream the FEL undulator system, they can also be used as diagnostics tools for the FEL pulse, allowing for calculating the pulse duration and even its spectrogram.

When the longitudinal phase space of an electron beam cannot be measured, it may be hard to optimize the accelerator parameters for lasing, e.g. for minimizing the radiation pulse duration. In this case one may resort to an analysis of the SASE FEL spectra. For example, based on the statistical properties of the radiation [5] one may apply spectral correlation analysis and estimate the average duration of the SASE FEL pulse assuming a certain temporal power profile [6, 7], further tuning the accelerator to decrease such duration by effect. However, the close relation between electron phase space and radiation characteristics must always be taken into account in this process. For example, it was shown in [8] that the chirp in an electron beam affects the range of spectral coherence, and hence the spectrum-based estimation of the SASE pulse duration.

Here we present a method to estimate duration and shape of SASE radiation pulses based on the reconstruction of autocorrelation of the ensemble-averaged pulse Wigner distribution. In Section 2 we discuss statistical properties of the SASE radiation, and show how the Wigner distribution autocorrelation can be calculated from measured SASE FEL spectra. In Section 3 we present SASE FEL spectra simulated with the FEL code GENESIS [9] assuming different electron beam parameters and we compare results of the reconstruction with known pulse shapes. Finally, in Section 4 we come to conclusions.

2 Theory

In this section we describe the theoretical background at the basis of our retrieval algorithm. We fix our notations and give several definitions. We then proceed to the formulation of the Wigner distribution autocorrelation reconstruction algorithm.

2.1 Definitions and conventions

Consider a scalar field $E(t)$ in the time domain and its Fourier transform $\bar{E}(\omega)$

$$\begin{aligned} \bar{E}(\omega) &= \frac{1}{2\pi}\int_{-\infty}^{\infty} dt\; E(t)\exp(i\omega t)\;, \\ E(t) &= \int_{-\infty}^{\infty} d\omega\; \bar{E}(\omega)\exp(-i\omega t)\;. \end{aligned} \tag{2}$$

We introduce the slowly varying field amplitude $\widetilde{E}(\omega)$ through the relation

$$\bar{E}(\omega) = \widetilde{E}(z,\omega)\exp(i\omega_c z/c)\;, \tag{3}$$

where ω_c is a central, carrier wavelength and z is the direction of propagation. Similarly to radiation power, measured single-shot spectra are proportional to the square-modulus of the single-shot slowly varying envelope

$$\begin{aligned} I(t) &\equiv E(t)E^*(t), \\ \widetilde{I}(\omega) &\equiv \widetilde{E}(\omega)\widetilde{E}^*(\omega)\;. \end{aligned} \tag{4}$$

The statistical autocorrelation function of the field $E(t)$ in the time domain can then be defined as[1]

$$\Gamma(t,\Delta t) = \left\langle E\left(t-\frac{\Delta t}{2}\right)E^*\left(t+\frac{\Delta t}{2}\right)\right\rangle, \tag{5}$$

where angle brackets $\langle\rangle$ denote ensemble average. The intensity autocorrelation function is, instead

$$\Gamma_I(t,\Delta t) = \left\langle I\left(t-\frac{\Delta t}{2}\right)I\left(t+\frac{\Delta t}{2}\right)\right\rangle\;. \tag{6}$$

The analogous correlation functions in the frequency domain are given by

$$\widetilde{\Gamma}(\omega,\Delta\omega) = \left\langle \widetilde{E}\left(\omega-\frac{\Delta\omega}{2}\right)\widetilde{E}^*\left(\omega+\frac{\Delta\omega}{2}\right)\right\rangle\;, \tag{7}$$

and

$$\widetilde{\Gamma}_I(\omega,\Delta\omega) = \left\langle \widetilde{I}\left(\omega-\frac{\Delta\omega}{2}\right)\widetilde{I}\left(\omega+\frac{\Delta\omega}{2}\right)\right\rangle\;. \tag{8}$$

It is also customary to define normalized correlation functions [5]. For example in the frequency domain:

$$\begin{aligned} \widetilde{g}_1(\omega,\Delta\omega) &= \frac{\left\langle \widetilde{E}\left(\omega-\Delta\omega/2\right)\widetilde{E}^*\left(\omega+\Delta\omega/2\right)\right\rangle}{\left\langle\left|\widetilde{E}\left(\omega-\Delta\omega/2\right)\right|^2\right\rangle^{1/2}\left\langle\left|\widetilde{E}\left(\omega+\Delta\omega/2\right)\right|^2\right\rangle^{1/2}} \\ &= \frac{\widetilde{\Gamma}(\omega,\Delta\omega)}{\sqrt{\left\langle\widetilde{I}\left(\omega-\Delta\omega/2\right)\right\rangle\left\langle\widetilde{I}\left(\omega+\Delta\omega/2\right)\right\rangle}} \end{aligned} \tag{9}$$

[1] Note that the autocorrelation function depends on both time t and time separation Δt, allowing to describe non-stationary radiation fields.

$$\widetilde{g_2}(\omega,\Delta\omega) = \frac{\left\langle \widetilde{I}(\omega-\Delta\omega/2)\widetilde{I}(\omega+\Delta\omega/2)\right\rangle}{\left\langle \widetilde{I}(\omega-\Delta\omega/2)\right\rangle\left\langle \widetilde{I}(\omega+\Delta\omega/2)\right\rangle} = \frac{\widetilde{\Gamma}_I(\omega,\Delta\omega)}{\left\langle \widetilde{I}(\omega-\Delta\omega/2)\right\rangle\left\langle \widetilde{I}(\omega+\Delta\omega/2)\right\rangle} \tag{10}$$

In order to characterize the radiation pulse in both domains, we consider a generalized class of time-frequency signal representations that was introduced by Cohen [10, 11]:

$$\begin{aligned} C(t,\omega) &= \frac{1}{4\pi^2}\iiint_{-\infty}^{\infty} d(\Delta\omega)d(\Delta t)du\ \ \Gamma(u,\Delta t)\phi(\Delta\omega,\Delta t)\exp(i\Delta\omega t + i\Delta t\omega - i\Delta\omega u) \\ &= \frac{1}{4\pi^2}\iiint_{-\infty}^{\infty} d(\Delta\omega)d(\Delta t)du\ \ \widetilde{\Gamma}(u,\Delta\omega)\phi(\Delta\omega,\Delta t)\exp(i\Delta\omega t + i\Delta t\omega - i\Delta\omega u) \end{aligned} \tag{11}$$

where $\phi(\Delta\omega,\Delta t)$ is a two-dimensional function called kernel [12] and determines the particular representation in the class.

Wigner distribution is one of the time-frequency representations, useful to describe properties of FEL radiation [13–17]:

$$\begin{aligned} \mathcal{W}(t,\omega) &= \frac{1}{2\pi}\int_{-\infty}^{\infty} d(\Delta t)\Gamma(t,\Delta t)\exp(i\omega\Delta t) \\ &= \int_{-\infty}^{\infty} d(\Delta\omega)\widetilde{\Gamma}(\omega,\Delta\omega)\exp(-i\Delta\omega t)\ . \end{aligned} \tag{12}$$

Its kernel $\phi(\Delta\omega,\Delta t) = 1$. Wigner distribution is real but can take negative values, and yields so called "cross terms" between signals in time-frequency plane. Nevertheless, when averaged over an ensemble, is positive for a great number of nonstationary processes which allows one to interpret it similarly to radiation spectrogram [18]. Its marginal distributions (projections on time and frequency domains) are radiation power and spectral power correspondingly:

$$\begin{aligned} \langle I(t)\rangle &= \int_{-\infty}^{\infty}\mathcal{W}(t,\omega)d\omega, \\ \left\langle \widetilde{I}(\omega)\right\rangle &= \int_{-\infty}^{\infty}\mathcal{W}(t,\omega)dt, \end{aligned} \tag{13}$$

Its first conditional moments of time and frequency are the instantaneous frequency and group delay:

$$\begin{aligned} \langle\omega\rangle_t &= \frac{1}{\langle I(t)\rangle}\int_{-\infty}^{\infty}\omega\mathcal{W}(t,\omega)d\omega, \\ \langle t\rangle_\omega &= \frac{1}{\left\langle \widetilde{I}(\omega)\right\rangle}\int_{-\infty}^{\infty}t\mathcal{W}(t,\omega)dt. \end{aligned} \tag{14}$$

The conditional spreads of Wigner distribution in frequency and time can also be introduced as instantaneous bandwidth and group delay spread

$$\sigma^2_{\omega|t} = \langle\omega^2\rangle_t - \langle\omega\rangle_t^2 = \frac{1}{\langle I(t)\rangle}\int_{-\infty}^{\infty}(\omega - \langle\omega\rangle_t)^2\,\mathcal{W}(t,\omega)d\omega,$$
$$\sigma^2_{t|\omega} = \langle t^2\rangle_\omega - \langle t\rangle_\omega^2 = \frac{1}{\left\langle\widetilde{I(\omega)}\right\rangle}\int_{-\infty}^{\infty}(t - \langle t\rangle_\omega)^2\,\mathcal{W}(t,\omega)dt, \tag{15}$$

alas, they may become negative, hence cannot always be properly interpreted [11, p.120].

Any representation of Cohen class can be expressed in terms of the Wigner distribution:

$$\begin{aligned} C(t,\omega) &= \frac{1}{2\pi}\iint_{-\infty}^{\infty} d(\Delta\omega)d(\Delta t)\;\; \Phi(\Delta t,\Delta\omega)\mathcal{W}(t-\Delta t,\omega-\Delta\omega) \\ &\equiv \frac{1}{2\pi}\Phi(\Delta t,\Delta\omega) ** \mathcal{W}(t-\Delta t,\omega-\Delta\omega), \end{aligned} \tag{16}$$

where

$$\Phi(t,\omega) = \frac{1}{2\pi}\iint_{-\infty}^{\infty} d(\Delta\omega)d(\Delta t)\phi(\Delta t,\Delta\omega)\exp(-i\Delta\omega t + i\Delta t\omega) \tag{17}$$

is just a different representation of Cohen kernel via its two-dimensional Fourier transform. Symbol $**$ denotes a two-dimensional convolution operator.

Spectrogram is another and much more known Cohen class function that facilitates time-frequency analysis:

$$S(t,\omega) = \left\langle\left|\frac{1}{\sqrt{2\pi}}\int_{-\infty}^{\infty} d\tau E(\tau)h(\tau - t)\exp(i\omega\tau)\right|^2\right\rangle. \tag{18}$$

It requires introduction of a window function $h(t)$ in time and frequency domain

$$H(\omega) = \frac{1}{\sqrt{2\pi}}\int_{-\infty}^{\infty} dt h(t)\exp(i\omega\tau). \tag{19}$$

Spectrogram kernel function is more complicated:

$$\phi(\Delta\omega,\Delta t) = \int_{-\infty}^{\infty} du\;\; h(u - \Delta t/2)h^*(u + \Delta t/2)\exp(i\Delta\omega u). \tag{20}$$

From Equations (16) and (17) it follows that the spectrogram of the signal f can be obtained by convolving the Wigner distribution W_f of that signal with the Wigner distribution W_h of the spectrogram window function h:

$$S_f(t,\omega) = W_f(t,\omega) ** W_h(-t,\omega), \tag{21}$$

in other words spectrogram is, in a way, a "smeared" version of the Wigner distribution. In contrast to a Wigner distribution, a spectrogram is non-negative everywhere, but it fails to yield radiation and spectral powers via its marginal distributions, as they are also "smeared" by being convolved with window functions:

$$\int_{-\infty}^{\infty} S(t,\omega)d(\omega) = \langle I(t)\rangle * |h(-t)|^2,$$
$$\frac{1}{2\pi}\int_{-\infty}^{\infty} S(t,\omega)d(t) = \left\langle \widetilde{I(\omega)}\right\rangle * |H(\omega)|^2 \tag{22}$$

If W_f is much "broader" than W_h (namely, the radiation pulse is far from its transform limit, or in other words, there are many spikes is the SASE spectrum), then the effect of "smearing" is negligible and both Wigner and spectrogram distributions are nearly indistinguishable and up to certain extent can be referred to interchangeably.

2.2 Stationarity, Ergodicity and SASE radiation

The electric field of a SASE FEL pulse as a function of time is a stochastic, or random, process. Generation of the field starts from the shot noise in an electron beam and yields quasimonochromatic radiation [1].

Let us consider a random process a where ${}^k a(t)$ is the value of the k-th realization of the variable a at time t. The finite time average of the k-th realization of $a(t)$ over time T is defined as

$$\left[{}^k a(t)\right]_T \equiv \frac{1}{T}\int_{t-T/2}^{t+T/2} {}^k a(t')dt' \ . \tag{23}$$

The full time-average of k-th realization is

$$\overline{{}^k a} = \lim_{T\to\infty}\left[{}^k a(t)\right]_T . \tag{24}$$

The ensemble average of the process a ig given by

$$\left\langle {}^k a(t)\right\rangle \equiv \frac{1}{N}\sum_{k=1}^{N} {}^k a(t). \tag{25}$$

We remind that stochastic processes can be separated into several broad classes [19, 20], illustrated on Figure 1.

In a **stationary** random process the probability distribution of any random variable or their combination does not depend on time. In a more narrowly defined **wide-sense stationary** random process, the ensemble-averages $\left\langle {}^k a(t)\right\rangle$ and $\left\langle {}^k a(t)^k a(t+\Delta t)\right\rangle$ are independent on t.

Finally, **ergodic** random process is the most restrictive subclass of stationary processes. It requires that any time average calculated over the sample function must be equal to the same average calculated over the ensemble:

$$\begin{aligned}
&\overline{{}^k a} = \langle {}^k a(t)\rangle, \\
&\overline{{}^k a(t)^k a(t+\Delta t)} = \langle {}^k a(t)^k a(t+\Delta t)\rangle. \\
&\ldots
\end{aligned} \tag{26}$$

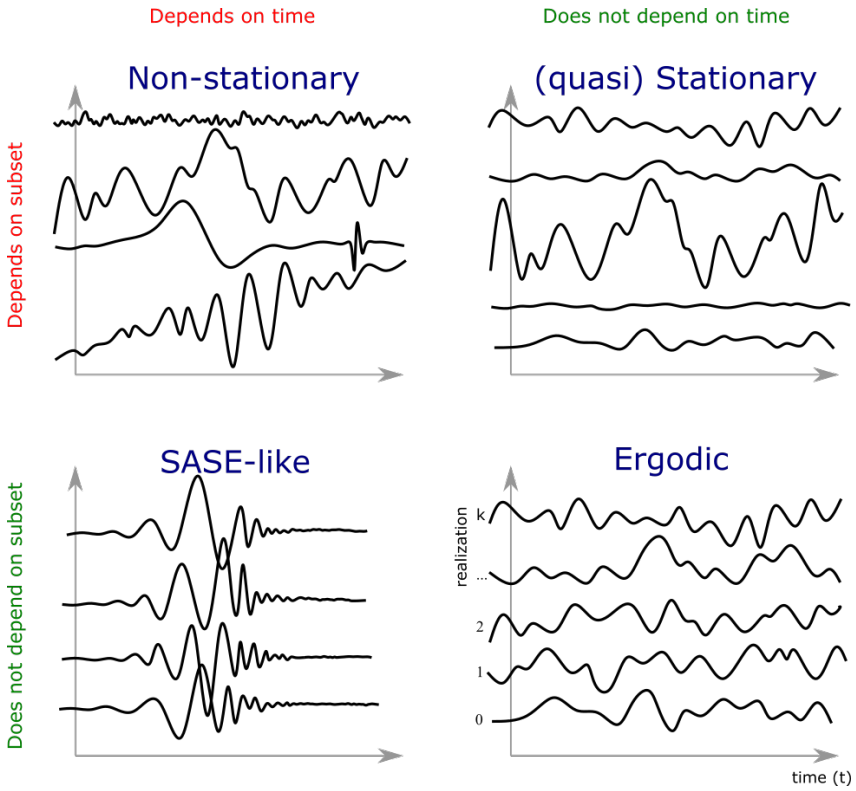

Figure 1: Statistical processes arranged according to whether their average depends on the choice of realization subset or the shift of time.

It follows from this definition that for ergodic processes the ensemble averages of any combination of random variables are defined and limited. This is not true for non-stationary or even stationary processes in a general case.

From these definitions it follows that any radiation field described by a stationary random process has no beginning, nor end, which strictly speaking is not physical. In order to avoid this issue, we call a process **quasistationary** when the finite time average of each realization $\left[{}^{k}a(t)\right]_T$ and its autocorrelation $\left[{}^{k}a(t)^{k}a(t+\Delta t)\right]_T$ are independent of time t.

An important property of *quasistationary* and *ergodic* processes is that their elsemble-averaged Wigner distribution (see Equation (12)) can be factorized, and therefore is non-negative [18]. This property is extremely useful for time-frequency analysis [21].

In principle, SASE FEL radiation in terms of its electric field value as a function of time in the time domain or as a function of frequency in the frequency domain can be categorized within the developed hierarchy of *non-stationary - stationary - ergodic processes* discussed above as a non-stationary process.

SASE radiation however exhibits an important property that distinguishes it from completely generic non-stationary processes: radiation power, instantaneous frequency and instantaneous bandwidth depend on electron beam slice properties, such as beam current, emittance, average and dispersion of electron energy, Twiss parameters, etc. The electron beam, in turn, is usually reproducible on a shot-to-shot basis, which means that the only random process involved in the radiation pulse generation is the intrinsic shot noise in the beam. This specific reproducibility of SASE radiation is illustrated on Figure 1.

Though the SASE generation process is both non-stationary and periodic, through the repetition rate of the electron beam, it should not be confused with *periodic non-stationary* process, discussed in [22, 23].

With examples from [18] in mind, we find empirically that the ensemble-averaged Wigner distribution of SASE FEL radiation pulses converges towards non-negative values (for an increasing number of realizations in ensemble) even when the Wigner distribution is not separable and not delineated in the time-frequency plane. This convergence is illustrated on Figures 2 and 3 where we present Wigner distributions of SASE FEL pulses, simulated with GENESIS code [9] and of their imitation, modeled with an algorithm presented in [24]. Postprocessing is carried out with OCELOT package [25]. In both cases the radiation has statistical properties of a Gaussian random process [19, sec. 3.1.4].

In contrast to convolution with window function to calculate non-negative spectrogram for every event, statistical averaging preserves correct marginals at the cost of losing single-shot information.

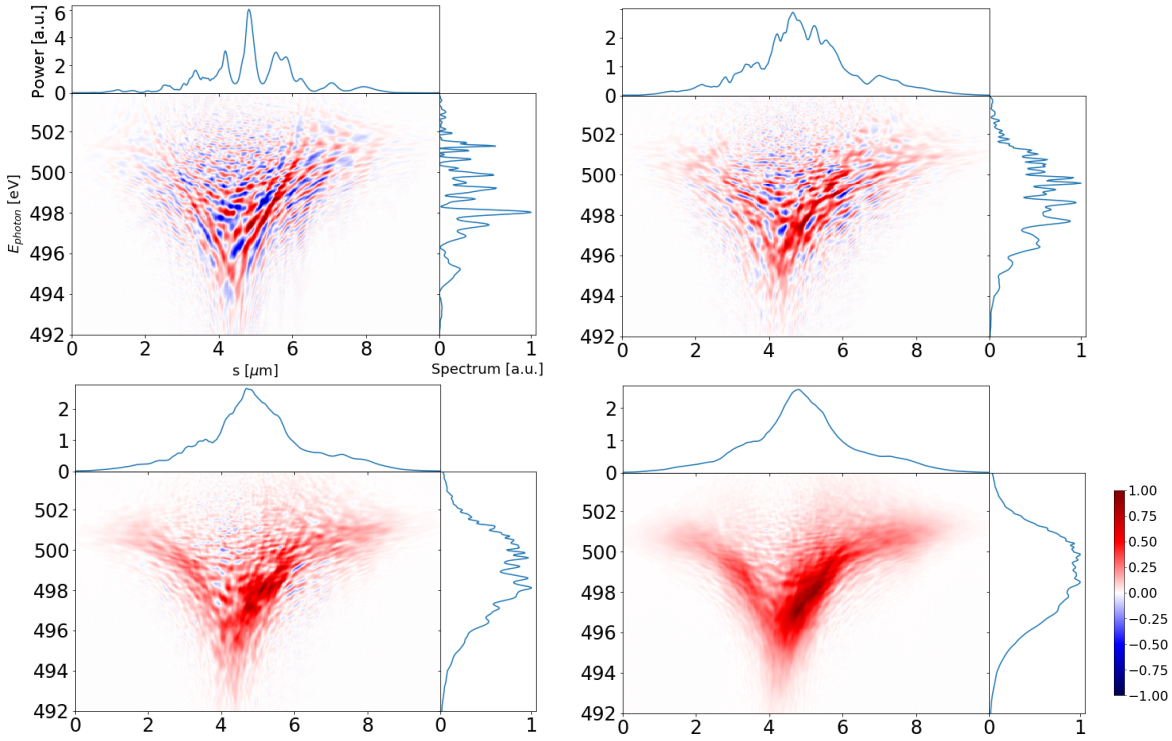

Figure 2: Colormap representations of the Wigner distribution of simulated SASE FEL radiation with their marginal distributions when averaged over an ensemble of one (upper left subfigure), 10 (upper right), 100 (lower left) and 1000 (lower right) statistically independent realizations. Note the significant non-linear frequency chirp in the pulse, visible upon ensemble averaging. Hereafter the diverging colormap of a Wigner distribution is normalized to its maximum absolute value, while its zero value is depicted with a white color.

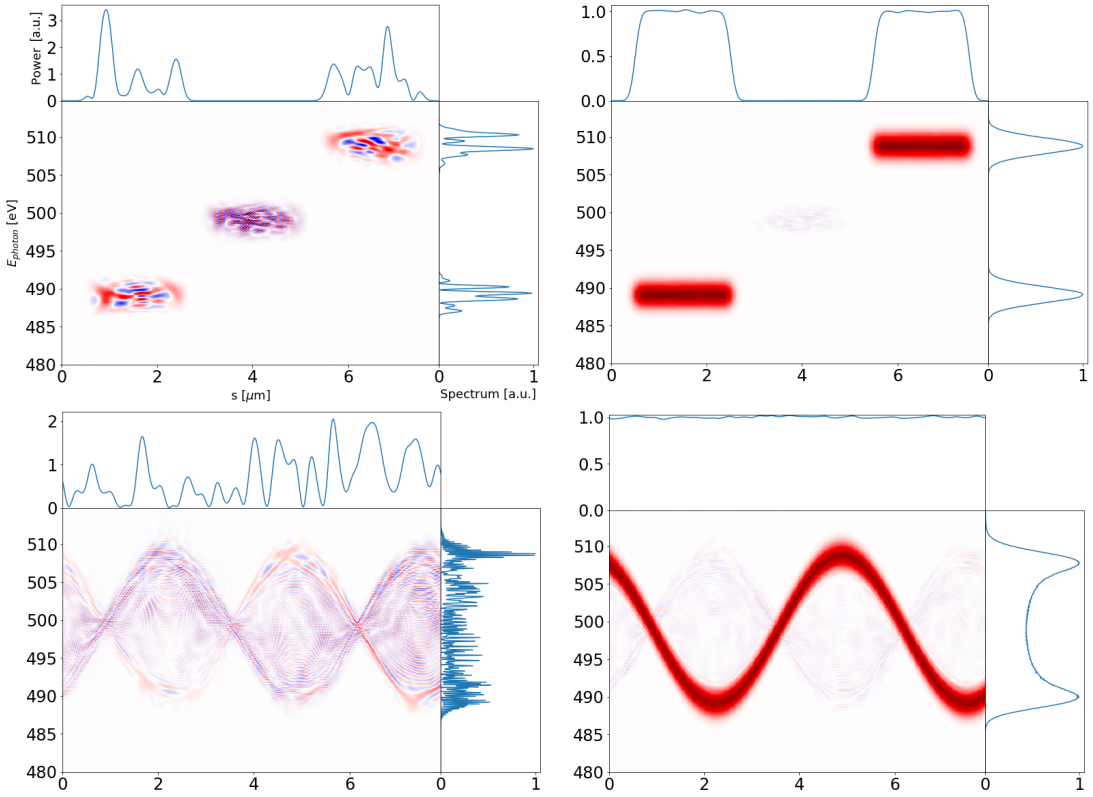

Figure 3: Colormap representations of the Wigner distribution of SASE FEL radiation imitation for two "flat-top" pulses with different frequencies (top subfigures) and for a continuous pulse with instantaneous frequency varying in time sinusoidally (bottom subfigures). The distributions averaged over an ensemble of one and 10000 statistically independent realizations are presented on the left and right subfigures correspondingly. The amplitude of the cross-terms is reduced significantly upon averaging over an ensemble.

2.3 Derivation of Wigner Distribution Autocorrelation

If we assume that scalar field $E(t)$ obeys Gaussian statistics, then the moment theorem for Gaussian random variables can be applied to the intensity autocorrelation function [19, sec. 8.4.1] to obtain:

$$\widetilde{\Gamma}_I(\omega, \Delta\omega) = \left\langle \widetilde{I}\left(\omega - \frac{\Delta\omega}{2}\right)\right\rangle \left\langle \widetilde{I}\left(\omega + \frac{\Delta\omega}{2}\right)\right\rangle + \left|\widetilde{\Gamma}(\omega, \Delta\omega)\right|^2 . \tag{27}$$

The latter is equivalent to the Siegert relation for normalized correlation functions

$$\widetilde{g}_2(\omega, \Delta\omega) = 1 + |\widetilde{g}_1(\omega, \Delta\omega)|^2. \tag{28}$$

This relation is valid for SASE radiation in both linear amplification regime and saturation [5, 6]. Let us now consider the following Fourier transform:

$$R(t, \omega) = \int_{-\infty}^{\infty} d(\Delta\omega) \left|\widetilde{\Gamma}(\omega, \Delta\omega)\right|^2 \exp(-i\Delta\omega t) . \tag{29}$$

Using the autocorrelation theorem we can equate

$$\begin{aligned}&\int_{-\infty}^{\infty} d(\Delta\omega)\left|\widetilde{\Gamma}(\omega,\Delta\omega)\right|^2 \exp(-i\Delta\omega t)\\&= \mathcal{A}\left[\int_{-\infty}^{\infty} d(\Delta\omega)\widetilde{\Gamma}(\omega,\Delta\omega)\exp(-i\Delta\omega t)\right],\end{aligned} \tag{30}$$

where $\mathcal{A}$ denotes autocorrelation, defined as it is generally done in signal processing[2]:

$$\mathcal{A}[f(t)] \equiv \int_{-\infty}^{\infty} f^*(\tau)f(t+\tau)d\tau\ . \tag{31}$$

We now note that the argument of the autocorrelation product in Equation (30) is the Wigner distribution function (which always has real values), and therefore

$$R(t,\omega) = \mathcal{A}\left[\mathcal{W}(t,\omega)\right] = \int_{-\infty}^{\infty} d\tau \mathcal{W}(\tau,\omega)\mathcal{W}(t+\tau,\omega)\ . \tag{32}$$

$R(t,\omega)$ is the autocorrelation of the Wigner distribution and can be directly calculated based on measured spectra of SASE FEL radiation. As discussed above, a Wigner distribution of such radiation becomes mostly positive upon averaging over sufficiently large statistical ensemble. Then it resembles a more known spectrogram distribution and can be analyzed accordingly. Hereinafter we refer to this function as the Reconstruction of Spectrogram Autocorrelation or for short, ROSA.

Another possible representation of the ROSA distribution for Gaussian wavefields can be derived:

$$R(t,\omega) = \mathcal{W}_y(t,\omega) - \int_{-\infty}^{\infty} d(\Delta t)\exp(i\omega\Delta t)\left\langle A\left[E(t-\Delta t/2)\right]\right\rangle\left\langle A^*\left[E(t+\Delta t/2)\right]\right\rangle\ , \tag{33}$$

where

$$y(t) = \int_{-\infty}^{\infty} E^*(\tau)E(t+\tau)d\tau = A[E(t)]\ . \tag{34}$$

ROSA distribution carries information on changes in temporal structure with frequency and vice versa. One of its properties is that its marginal distribution on the frequency domain yields the square of the average radiation spectrum.

$$\begin{aligned}\int_{-\infty}^{\infty} dt R(t,\omega) &= \int_{-\infty}^{\infty} d\tau \mathcal{W}(\tau,\omega)\left[\int_{-\infty}^{\infty} dt \mathcal{W}(t+\tau,\omega)\right]\\&= \int_{-\infty}^{\infty} d\tau \mathcal{W}(\tau,\omega)\langle\widetilde{I}(\omega)\rangle = 4\pi^2\langle\widetilde{I}(\omega)\rangle^2\ ;\end{aligned} \tag{35}$$

Projection in another direction can be derived:

$$\begin{aligned}\int_{-\infty}^{\infty} d\omega R(t,\omega) &= \int_{-\infty}^{\infty} d\omega \mathcal{W}_y(t,\omega)\\&\quad - \int_{-\infty}^{\infty} d\omega\exp(i\omega\Delta t)\int_{-\infty}^{\infty} d(\Delta t)\left\langle A\left[E(t-\Delta t/2)\right]\right\rangle\left\langle A^*\left[E(t+\Delta t/2)\right]\right\rangle\\&= 2\pi\left[\left\langle\left|A\left[E(t)\right]\right|^2\right\rangle - \left\langle\left|A\left[E(t)\right]\right|\right\rangle^2\right] \equiv 2\pi\sigma^2\left[\left|A\left[E(t)\right]\right|\right]\ ,\end{aligned} \tag{36}$$

[2]Statistical definition of the autocorrelation function is different

where $\sigma^2[f(t)]$ is variance of a function f. A cut $R(t, \omega = const)$ therefore gives a certain correlation-like function of the field after bandpass filter at frequency ω.

2.4 ROSA Algorithm

The algorithm of reconstruction of the spectrogram autocorrelation is very simple and consists of the following conceptual steps.

First, sufficiently large statistics of single shot SASE FEL spectra, in the form of Eq. (4) is acquired. Here we assume that only SASE-related fluctuations are present. Otherwise, the measured data should be filtered since they are prone to additional jitter, unrelated to the SASE process.

Second, we calculate the quantity

$$\begin{aligned} Q(\omega, \Delta\omega) &\equiv \left|\widetilde{\Gamma}(\omega, \Delta\omega)\right|^2 \\ &= \left\langle \widetilde{I}\left(\omega - \frac{\Delta\omega}{2}\right)\widetilde{I}\left(\omega + \frac{\Delta\omega}{2}\right)\right\rangle - \left\langle \widetilde{I}\left(\omega - \frac{\Delta\omega}{2}\right)\right\rangle \left\langle \widetilde{I}\left(\omega + \frac{\Delta\omega}{2}\right)\right\rangle . \end{aligned} \tag{37}$$

Finally, third, an inverse Fourier transform yields the reconstruction function R:

$$R(t, \omega) = \int_{-\infty}^{\infty} d(\Delta\omega) Q(\omega, \Delta\omega) \exp(-i\Delta\omega t) . \tag{38}$$

We have found that binning of reconstruction function R over several points in both dimensions greatly reduces numerical noise with practically no cost for effective resolution. This binning effectively serves as convolution of Wigner distribution of the signal with that of a window function, as in Equation (21), with its consecutive desampling.

2.5 Factorization of quasistationary pulses

Let us see what simplifications arise if the considered Gaussian process is also quasistationary. The assumption of quasi-stationarity allows us to neglect the dependence of the normalized correlation functions on central frequency ω i.e. they depend only on frequency separation: $g_1(\Delta\omega), g_2(\Delta\omega)$.

This allows one to factorize autocorrelation functions

$$\widetilde{\Gamma}(\omega, \Delta\omega) = \left\langle \widetilde{I}(\omega)\right\rangle \widetilde{g}_1(\Delta\omega) , \tag{39}$$

$$\widetilde{\Gamma}_I(\omega, \Delta\omega) = \left\langle \widetilde{I}(\omega)\right\rangle^2 \widetilde{g}_2(\Delta\omega) \tag{40}$$

and, consequently the reconstruction function,

$$R(t, \omega) = \left\langle \widetilde{I}(\omega)\right\rangle^2 \mathcal{A}\left[\langle I(t)\rangle\right] . \tag{41}$$

By integrating over frequencies, or fixing any value $\omega = \omega_0$, we see that the reconstructed function $\int_{-\infty}^{\infty} R(t, \omega) d\omega$ or, alternatively, $R(t, \omega_0)$ is simply, aside for an unimportant multiplicative constant, the autocorrelation of the FEL pulse power in the time domain.

2.6 Analogy with the Wiener-Khinchin theorem

Here we discuss an interesting analogy between Equation (29) and the famous Wiener-Khinchin theorem. The Wiener-Khinchin theorem plays a central role in Fourier-transform spectroscopy and allows one to calculate the radiation spectral density after directly measuring the amplitude autocorrelation function of the radiation in the time domain. We remind that the this theorem holds for wide-sense stationary processes and can be formulated, mathematically, as:

$$\langle \widetilde{I}(\omega) \rangle = \frac{1}{2\pi} \int_{-\infty}^{\infty} d(\Delta t)\, \Gamma(\Delta t) \exp(i\omega \Delta t)\ . \tag{42}$$

It states that the statistical autocorrelation function of a stationary random process in the *time* domain and the ensemble-averaged spectral density, i.e. power spectrum, of that process form a Fourier transform pair.

Should the process be quasi-stationary, a similar relation would naturally hold between the autocorrelation function in the *frequency* domain and the ensemble-averaged intensity, or pulse shape, in the time domain:

$$\langle I(t) \rangle = \int_{-\infty}^{\infty} d(\Delta\omega)\, \widetilde{\Gamma}(\Delta\omega) \exp(-i\Delta\omega t)\ . \tag{43}$$

One can now see the similarity between Equations (43) and (29). The latter is simply the combination of the autocorrelation theorem and the Wiener-Khinchin theorem applied in the opposite domain.

In Fourier-transform spectroscopy the *time* autocorrelation function Γ is obtained by carrying average over time, as the investigated process is assumed to be ergodic. This averaging naturally leads to the loss of the dependence of the function Γ from time, so one obtains the statistical autocorrelation function of time delay $\Gamma(\Delta t)$ over which the Fourier transform is later performed.

In our case, the *statistical* frequency autocorrelation function $\widetilde{\Gamma}(\omega, \Delta\omega)$ is calculated via averaging over an ensemble of single-shot spectra. Such averaging is justified by statistical properties of SASE radiation, discussed in Section 2.2. Dependence on both central frequency ω and frequency difference $\Delta\omega$ remains, yielding additional information upon Fourier transform over $\Delta\omega$.

3 Numerical simulations and discussions

In order to illustrate the performance of ROSA, we simulated four ensembles of FEL spectra with the FEL code GENESIS [9] and analyzed them with the OCELOT package [25, 26]. We generated 500 statistically independent SASE events assuming a model 6μm-long flattop electron beams with (i) and without (ii) energy chirp. Also we simulated SASE generation by two 2μm-long flattop electron beams separated by 3 micrometers (iii). Finally, 1000 statistically independent SASE events assuming a nominal 100pC electron beam from s2e simulations for the European XFEL (iv) [27, 28]. The slice properties of the model beams are chosen to be close to those of the 100 pC nominal electron beam. The radiation generated by model beams was dumped before saturation to reduce the radiation slippage and maintain the illustrative flat-top

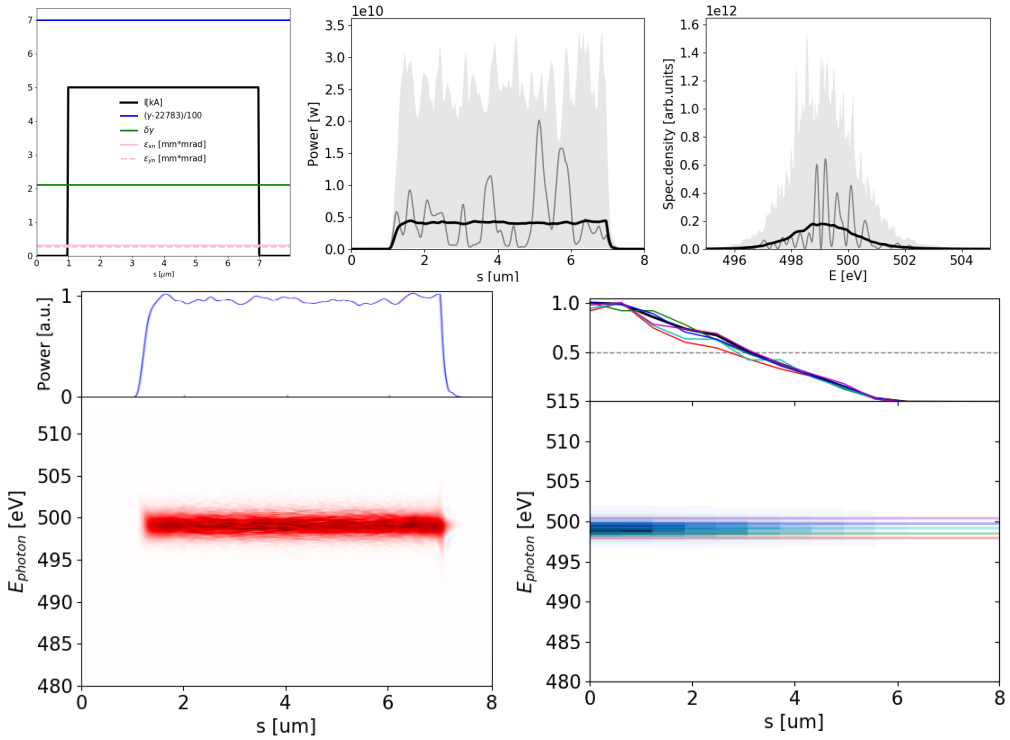

Figure 4: A 6μm-long flattop model electron beam without energy chirp, see top left plot, was used to generate SASE radiation. It was dumped during the exponential growth. Power and spectra of 500 statistically independent events are presented on the middle and on the right top plots correspondingly. The ensemble-averaged Wigner distribution of the SASE radiation is presented on the bottom left plot. The spectrogram autocorrelation reconstruction $R(ct, \hbar\omega/e)$ is presented on the bottom right plot.

distribution of the ensemble-averaged radiation power. The realistic 100 pC beam radiation was dumped, instead, in deep saturation.

The bottom left plots in Figures 4 and following present the ensemble-averaged Wigner distribution of the radiation. This distribution is based on information about amplitudes and phases of SASE radiation provided by simulation and is used here to assess representativeness of the bottom right plot. The latter depicts the ROSA function, calculated with Equation (29). The colored line-offs allow one to compare the reconstructed spectrogram autocorrelation at the various photon energies. The reconstruction is symmetrical with respect to coordinate s, hence only a half of it is depicted.

If no energy chirp is present in the electron beam, the undulator resonance condition is constant along the beam and the generated radiation pulse has no frequency chirp (Figure 4). In this special case the Wigner distribution, and hence the reconstruction, are factorisable (Equation (41)) and the total pulse length can be estimated: the autocorrelation of the flat-top power profile with length Δs would yield an autocorrelation result with triangular shape and full width at half maximum (fwhm) equal to $\Delta s/2$. In the case of a Gaussian radiation pulse with fwhm Δs, the fwhm size of its autocorrelation result will be $\sqrt{2}\Delta s$.

When the energy chirp in the electron beam (i.e. the relative difference of electron energy in the head and tail) exceeds FEL efficiency parameter $\Delta\gamma/\gamma \gtrsim \rho$, a frequency chirp along SASE pulse can be observed. As a consequence it will yield a broader

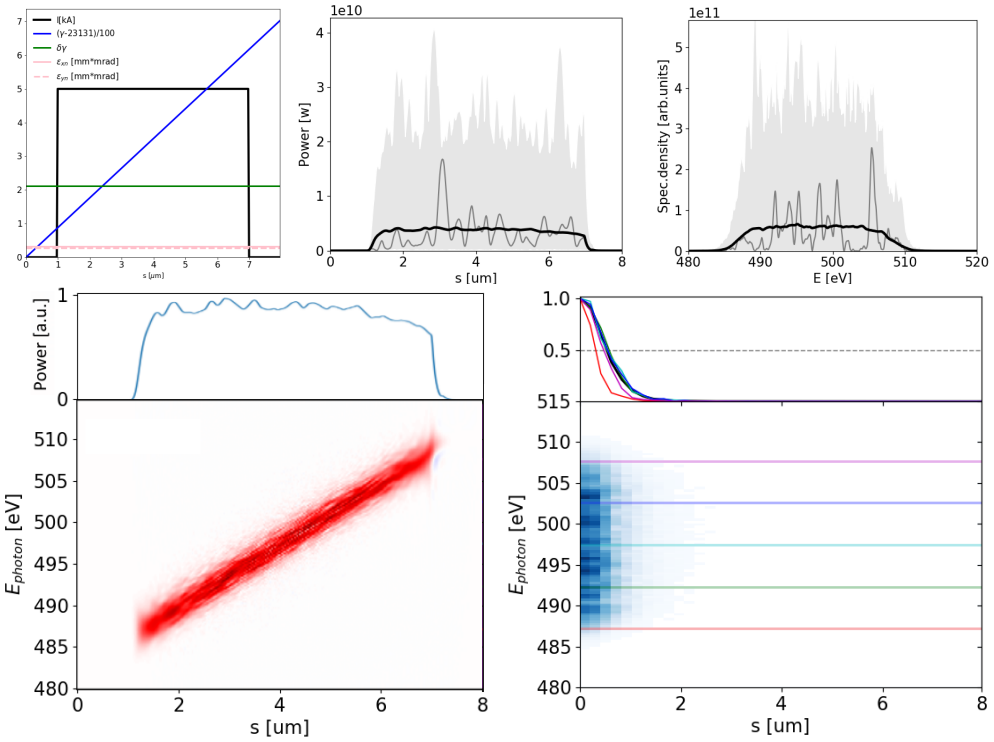

Figure 5: See plots descriptions from Figure 4, except in this case the linear energy chirp is introduced to the electron beam.

spectrum (which is the integral of the Wigner distribution over time) and typically a shorter pulse length at all photon energies [8] (horizontal line-offs of the Wigner distribution), as presented on Figure 5. These effects are also reflected in the spectral correlation functions, and, if not accounted for, an underestimation of the total pulse duration will take place.

Two sequential radiation pulses with equal carrier frequencies, separated by time Δt will yield a spectrum with modulated amplitude. The spectral modulation period is given by

$$\delta E\ [eV] = 10^6 \frac{hc}{e\Delta s\ [\mu m]} \simeq \frac{1.240}{\Delta s\ [\mu m]} \simeq \frac{4.135}{\Delta t\ [fs]}$$

where h is the Planck's constant, c is speed of light, e is the electron charge, s and t are the pulse separations in space (micrometers) and time (femtoseconds) correspondingly. The discussed modulation of spectral density takes place only at the frequencies common for both pulses, therefore if individual spectra of the two pulses do not have common frequencies, i.e. do not overlap in the frequency domain, no "beating" in this domain will take place.

Similarly, the SASE spectra obtained from two model flat-top electron beams with equal energies are expected to be modulated. If a spectrometer is capable of resolving this modulation, one can estimate their temporal separation. This scenario is exemplified on Figure 6. Since the SASE spectra are already intrinsically "spiky", it is not easy to discover additional modulation just upon visual examination. However, the spectral correlation function clearly indicates the correlation between the maxima in the spectrum (see Figure 7). The latter does not take place for statistically independent SASE modes.

Note, that both the Wigner distribution and the reconstruction indicate equal tem-

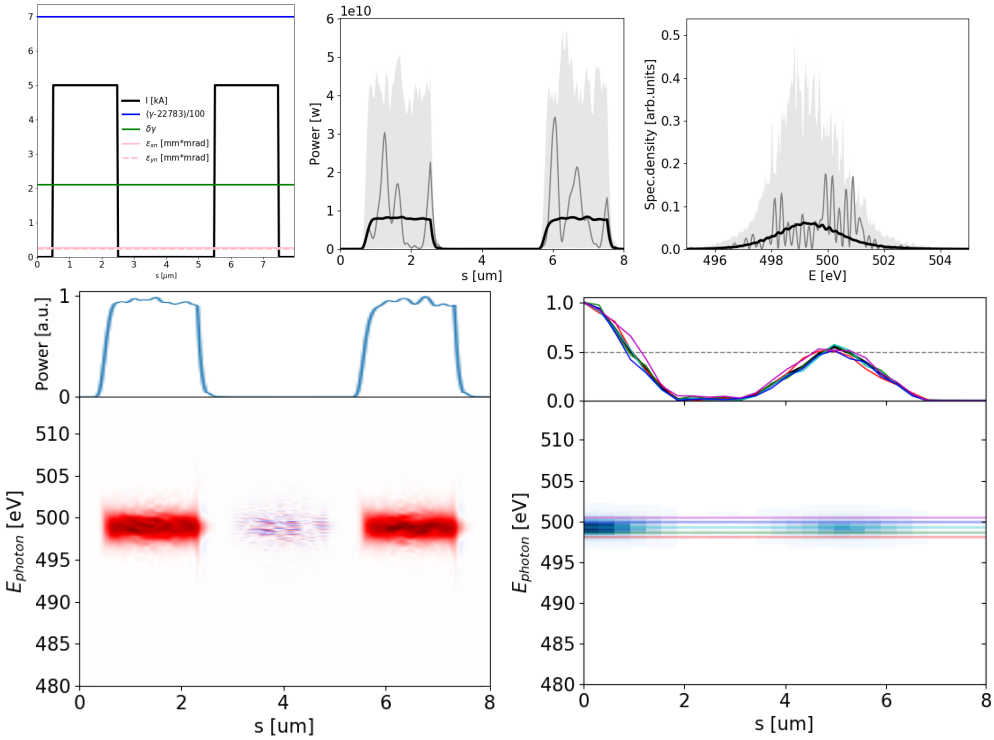

Figure 6: See plots descriptions from Figure 4. Here two flat-top 2 μm-long electron beams, separated by 3 μm, generate two consecutive SASE pulses of the same averaged shape.

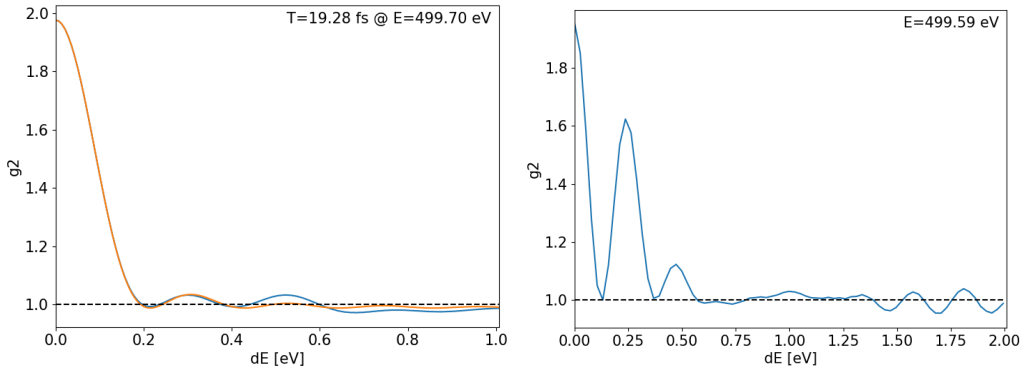

Figure 7: Normalized second-order spectral correlation functions g_2. The left plot corresponds to the single radiation pulse discussed on Figure 4; the right plot corresponds to the two pulses on Figure 6. In the case of the 6 μm-long radiation pulse with flattop averaged power profile, we fit the function g_2 with a theoretical shape corresponding to the pulse duration of 19.3 fs.

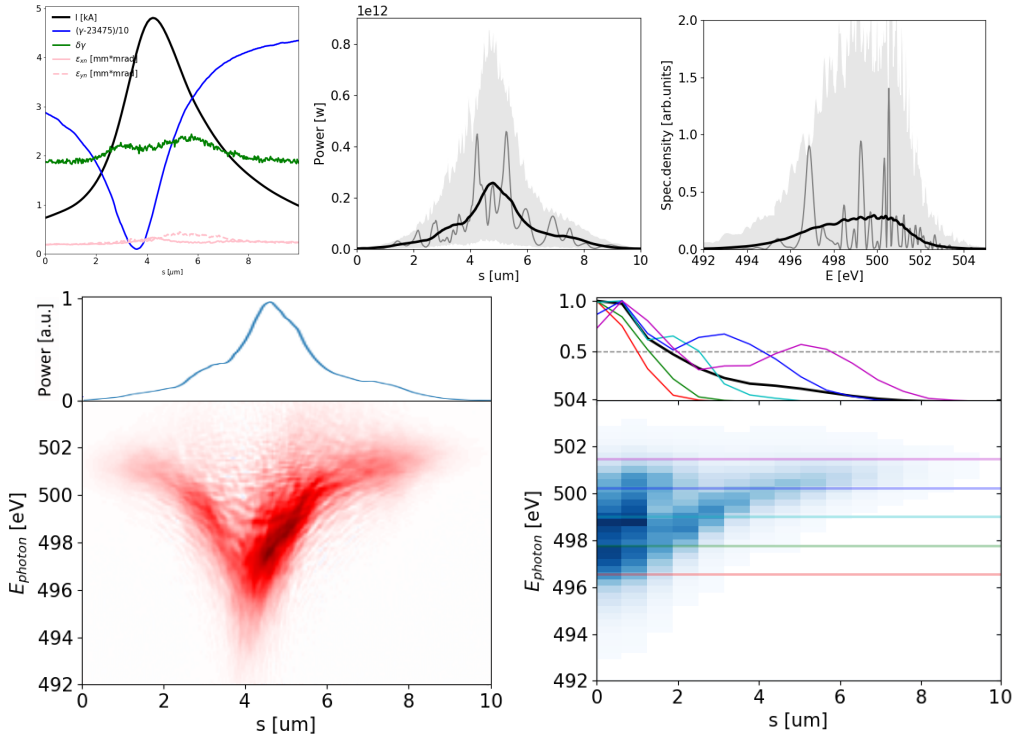

Figure 8: See plots descriptions from Figure 4. The nominal European XFEL 100pC electron beam with a non-linear energy chirp produces SASE radiation with different durations at different photon energies. Note the bifurcation in Wigner distribution above 499 eV. Analysis based on 1000 simulated SASE spectra

poral separation between SASE pulse centers — 5 μm or 16.5 fs — at all photon energies.

In general, the electron beam formation system may yield a highly non-linear energy chirp, as illustrated on Figure 8 (top left plot). If the relative peak-to-valley energy difference in the electron beam is comparable or larger than a Pierce parameter ρ, the electron beam energy chirp will be imprinted into the SASE radiation spectrogram as a radiation frequency chirp. In the given example two distinct pulses separated by about 6 μm at 501 eV photon energy are visible on the radiation spectrogram. The separation of these "double pulses" grows with the photon energy, following the separation of the electron beam slices with an equal Lorenz factor γ. Similarly to the double-pulse case, illustrated in Figure 6, such photon-energy-dependent separation can be straightforwardly observed in the reconstruction function

Our spectrum-based pulse length estimation is a zero-cost, effective diagnostics that does not require any hardware aside for a high-resolution single-shot spectrometer, which is typically available at XFEL facilities. It relies upon the fact that the FEL pulses are short, narrow-bandwidth, and follow Gaussian statistics, strictly in the linear regime, and approximatively at saturation [6]. The conventional method of fitting the experimental second-order spectral correlation function of SASE radiation with the theoretical one requires an initial assumption on the power profile of the SASE pulse [6, 7]. Also, if an energy chirp is present in the electron beam, the fitting will yield an underestimated pulse duration.

We suggest that in many cases, the analysis of a radiation spectrogram by means of its temporal autocorrelation may be more straightforward and less misleading,

especially when no information about the electron beam longitudinal phase space is available due to lack of an XTCAV system installed after the SASE undulator.

4 Conclusions

We discussed several statistical properties of SASE FEL radiation that allow us to define an ensemble-averaged Wigner distribution; we find empirically that it tends to become everywhere positive therefore very useful for time-frequency analysis of SASE FEL radiation.

We present an extend method to analyze the temporal SASE radiation properties. We show that based on the second order spectral correlation function it is possible to calculate a $R(t, \omega)$ - an autocorrelation of the ensemble-averaged Wigner distribution of the radiation. The latter, upon noise filtering via binning, is close in terms of its properties to the well-known spectrogram distribution. Therefore, we call the proposed method ROSA: Reconstruction of Spectrogram Autocorrelation.

The proposed method allows one to estimate the average group spread in the pulse, i.e. the pulse length individually for all photon energies in the pulse, to indicate the presence of two FEL pulses with overlapping spectra and to estimate their duration and temporal separation. This method is statistical in nature and relies upon the assumption that FEL hardware provides a reproducible electron beam along the stable orbit. Otherwise, discrimination of outlier events should take place.

We simulated 500 statistically independent SASE events assuming a model 6μm-long flattop electron beams with (i) and without (ii) energy chirp. Also we simulated SASE generation by two 2μm-long flattop electron beams separated by 3 micrometers (iii). Finally, 1000 statistically independent SASE events assuming a nominal 100pC electron beam from s2e simulations for the European XFEL (iv) [28]. Simulation results allowed us to compare the apriori known Wigner distributions with calculated ROSA distributions.

We provided an intuitive understanding of advantages and limitations of ROSA algorithm. Some limitations, like the inability to provide the total pulse duration in the presence of a significant energy chirp in the electron beam without additional knowledge, are common for the all methods based on spectral correlation function analysis.

5 Acknowledgments

We would like to thank Guenter Brenner, Stefan Duesterer, Bart Faatz, Jan Gruenert, Vitaly Kocharyan, Naresh Kujala, Jia Liu, Juliane Roensch-Schulenburg, Evgeny Saldin, Takanori Tanikawa, Sergey Tomin, Mikhail Yurkov for useful discussions and Serguei Molodtsov for his interest in this work.

References

[1] E. Saldin, E. Schneidmiller, and M. Yurkov. *The Physics of Free Electron Lasers*. Springer Berlin Heidelberg, 2010. ISBN: 9783642085550. URL: https://link.springer.com/book/10.1007/978-3-662-04066-9.

[2] B. W. J. McNeil and N. R. Thompson. "X-ray free-electron lasers". In: *Nat. Photonics* 4.12 (2010), pp. 814–821. ISSN: 1749-4885. DOI: 10.1038/nphoton.2010.239.

[3] C. Pellegrini, A. Marinelli, and S. Reiche. "The physics of x-ray free-electron lasers". In: *Rev. Mod. Phys.* 88.1 (2016), p. 015006. ISSN: 0034-6861. DOI: 10.1103/RevModPhys.88.015006.

[4] C. Behrens et al. "Few-femtosecond time-resolved measurements of X-ray free-electron lasers". In: *Nat. Commun.* 5.1 (2014), p. 3762. ISSN: 2041-1723. DOI: 10.1038/ncomms4762.

[5] E. Saldin, E. Schneidmiller, and M. Yurkov. "Statistical properties of radiation from VUV and X-ray free electron laser". In: *Opt. Commun.* 148.4-6 (1998), pp. 383–403. ISSN: 00304018. DOI: 10.1016/S0030-4018(97)00670-6.

[6] A. A. Lutman et al. "Femtosecond x-ray free electron laser pulse duration measurement from spectral correlation function". In: *Phys. Rev. Spec. Top. - Accel. Beams* 15.3 (2012), p. 030705. ISSN: 1098-4402. DOI: 10.1103/PhysRevSTAB.15.030705.

[7] Y. Inubushi et al. "Determination of the Pulse Duration of an X-Ray Free Electron Laser Using Highly Resolved Single-Shot Spectra". In: *Phys. Rev. Lett.* 109.14 (2012), p. 144801. ISSN: 0031-9007. DOI: 10.1103/PhysRevLett.109.144801.

[8] S. Krinsky and Z. Huang. "Frequency chirped self-amplified spontaneous-emission free-electron lasers". In: *Phys. Rev. Spec. Top. - Accel. Beams* 6.5 (2003), pp. 11–17. ISSN: 10984402. DOI: 10.1103/PhysRevSTAB.6.050702.

[9] S. Reiche. "GENESIS 1.3: A fully 3D time-dependent FEL simulation code". In: *Nucl. Instruments Methods Phys. Res. Sect. A Accel. Spectrometers, Detect. Assoc. Equip.* 429.1 (1999), pp. 243–248. ISSN: 01689002. DOI: 10.1016/S0168-9002(99)00114-X.

[10] L. Cohen. "Generalized Phase-Space Distribution Functions". In: *J. Math. Phys.* 7.5 (1966), pp. 781–786. ISSN: 0022-2488. DOI: 10.1063/1.1931206.

[11] L. Cohen. *Time Frequency Analysis: Theory and Applications*. New Jersey: A Pearson Education Company, 1995. ISBN: 0-13-594532-1.

[12] T. A.C. M. Claasen and W. F. Mecklenbrauker. "The wigner distribution - a tool for time-frequency signal analysis". In: *Philips J. Res.* 35.6 (1980), pp. 372–389. ISSN: 01655817. URL: http://www.extra.research.philips.com/hera/people/aarts/{_}PhilipsBoundArchive/PJR/PJR-35-1980-372.pdf.

[13] J. Wu et al. "Interplay of the chirps and chirped pulse compression in a high-gain seeded free-electron laser". In: *J. Opt. Soc. Am. B* 24.3 (2007), p. 484. ISSN: 0740-3224. DOI: 10.1364/JOSAB.24.000484.

[14] E Allaria et al. "The FERMI@Elettra free-electron-laser source for coherent x-ray physics: photon properties, beam transport system and applications". In: *New J. Phys.* 12.7 (2010), p. 075002. ISSN: 1367-2630. DOI: 10.1088/1367-2630/12/7/075002.

[15] G. Marcus, G. Penn, and A. A. Zholents. "Free-Electron Laser Design for Four-Wave Mixing Experiments with Soft-X-Ray Pulses". In: *Phys. Rev. Lett.* 113.2 (2014), p. 024801. ISSN: 0031-9007. DOI: 10.1103/PhysRevLett.113.024801.

[16] S. Huang et al. "Generation of subterawatt-attosecond pulses in a soft x-ray free-electron laser". In: *Phys. Rev. Accel. Beams* 19.8 (2016), pp. 1–7. ISSN: 24699888. DOI: 10.1103/PhysRevAccelBeams.19.080702.

[17] S. Serkez. "Self-Seeding XFELs: Operation Principle and Challenges". In: *Synchrotron Radiat. News* 29.3 (2016), pp. 10–14. ISSN: 19317344. DOI: 10.1080/08940886.2016.1174037.

[18] P. Flandrin. "On the positivity of the Wigner-Ville spectrum". In: *Signal Processing* 11.2 (1986), pp. 187–189. ISSN: 01651684. DOI: 10.1016/0165-1684(86)90037-X.

[19] L. Mandel and E. Wolf. *Optical Coherence and Quantum Optics*. Cambridge, 1995. ISBN: 0521417112.

[20] J. W. Goodman. *Statistical optics*. New York: John Wiley & Sons, 2000. ISBN: 0-47 1-0 1502-4.

[21] A. Janssen and T. Claasen. "On positivity of time-frequency distributions". In: *IEEE Trans. Acoust.* 33.4 (1985), pp. 1029–1032. ISSN: 0096-3518. DOI: 10.1109/TASSP.1985.1164622.

[22] H. Ogura. "Spectral representation of a periodic nonstationary random process". In: *IEEE Trans. Inf. Theory* 17.2 (1971), pp. 143–149. ISSN: 0018-9448. DOI: 10.1109/TIT.1971.1054612.

[23] W. Gardner and L. Franks. "Characterization of cyclostationary random signal processes". In: *IEEE Trans. Inf. Theory* 21.1 (1975), pp. 4–14. ISSN: 0018-9448. DOI: 10.1109/TIT.1975.1055338.

[24] T. Pfeifer et al. "Partial-coherence method to model experimental free-electron laser pulse statistics". In: *Opt. Lett.* 35.20 (2010), p. 3441. ISSN: 0146-9592. DOI: 10.1364/OL.35.003441.

[25] I. Agapov et al. *Ocelot collaboration webpage*. URL: https://github.com/ocelot-collab/ocelot.

[26] I. Agapov et al. "OCELOT: A software framework for synchrotron light source and FEL studies". In: *Nucl. Instruments Methods Phys. Res. Sect. A Accel. Spectrometers, Detect. Assoc. Equip.* 768 (2014), pp. 151–156. ISSN: 01689002. DOI: 10.1016/j.nima.2014.09.057.

[27] M. Altarelli and Others. *The European X-ray Free-Electron Laser*. Tech. rep. July. European XFEL, 2006. URL: http://xfel.desy.de/tdr/tdr.

[28] I. Zagorodnov. *DESY MPY Start-to-End Simulations page: http://www.desy.de/fel-beam/s2e/xfel.html*. URL: http://www.desy.de/fel-beam/s2e/xfel.html.